

Detectability of the 21 cm-CMB cross-correlation from the EoR

Hiroyuki Tashiro¹, Nabila Aghanim¹, Mathieu Langer¹,
Marian Douspis¹, Saleem Zaroubi², and Vibor Jelic²

¹ *Institut d'Astrophysique Spatiale (IAS), Bâtiment 121, Université Paris-Sud XI and CNRS, F-91405, Orsay (France);*

² *Kapteyn Astronomical Institute, University of Groningen, Postbus 800, NL-9700AV, Groningen, (The Netherlands)*

22 February 2024

ABSTRACT

The 21-cm line fluctuations and the cosmic microwave background (CMB) are powerful probes of the epoch of reionisation (EoR) of the universe. We study the potential of the cross-correlation between 21-cm line fluctuations and CMB anisotropy to obtain further constraints on the reionisation history. We compute analytically the 21-cm cross-correlation with the CMB temperature anisotropy and polarisation, and we calculate the signal-to-noise (SN) ratio for its detection with *Planck* together with LOFAR, MWA and SKA. We find, on the one hand, that the 21-cm cross-correlation signal with CMB temperature from the instant reionisation can be detected with an SN ratio of ~ 2 for LOFAR and ~ 10 for SKA. On the other hand, we confirm that the detection of the 21-cm cross-correlation with CMB polarisation is practically infeasible.

Key words: cosmology: theory – cosmic microwave background – large-scale structure of universe

1 INTRODUCTION

The measurement of 21 cm line of neutral hydrogen from high redshifts is eagerly awaited as a probe of the Epoch of Reionisation (EoR). During the EoR, the first collapsed objects heat and ionise the intergalactic medium (IGM). Therefore, the epoch and the process of reionisation are tightly related to the evolution of cosmological structure and the formation of the first objects (Barkana & Loeb 2001; Ciardi & Ferrara 2005; Fan et al. 2006). The 21 cm fluctuations are sensitive to the density, temperature, and ionised fraction of IGM. Studying the 21-cm tomography tells us about the physics of IGM gas and structure formation during the EoR (Madau et al. 1997; Tozzi et al. 2000; Ciardi & Madau 2003; Furlanetto et al. 2004), and several 21-cm experiments are recently designed and built (e.g. MWA¹, LOFAR², SKA³).

The 21 cm cross-correlation with other complementary probes is expected to provide additional information other than their respective auto-correlations. Besides, the cross-correlation has an advantage for observations of 21 cm fluctuations whose signal is weak, because it suffers from foregrounds and systematic effects less than the auto-correlations. The cross-correlation between the 21 cm line and the cosmic microwave background (CMB) has been studied by many authors. On large scales ($\ell \sim 100$), the 21-cm fluctuations cross-correlate with the CMB Doppler temperature anisotropies which are due to the motions of ionised baryons (Alvarez et al. 2006; Adshead & Furlanetto 2007). Because the maximum amplitude of the cross-correlation is reached at the redshift when the ionised fraction is one half, it is sensitive to the EoR. On small scales ($\ell > 1000$), cross-correlation between the 21 cm fluctuations and CMB temperature anisotropies from reionisation bubbles arises (Salvaterra et al. 2005; Cooray 2004; Slosar et al. 2007; Jelic et al. 2009). Salvaterra et al. (2005) showed that these two signals are anti-correlated on the scale corresponding to the typical size of an ionised bubble. Tashiro et al. (2008) studied the 21 cm cross-correlation with CMB *E*-mode polarisation on large scales. They have shown that the peak of the cross-correlation spectrum reaches its maximum value when the average ionised fraction of the universe is about half as shown in the case of

¹ <http://web.haystack.mit.edu/array/MWA>

² <http://www.lofar.org>

³ <http://www.skatelescope.org>

the 21 cm cross-correlation with the CMB Doppler temperature, and there is a damping that depends on the duration of reionisation. The cross-correlation between the 21 cm fluctuations and high redshift galaxy distribution has also the potential to probe the EoR (Wyithe & Loeb 2007; Furlanetto & Lidz 2007; Lidz et al. 2009). On large scales, the 21-cm and galaxy distributions are anti-correlated, while on scales smaller than the typical size of an ionised bubble, these fields become roughly uncorrelated. Therefore, the cross-correlation between the 21 cm fluctuations and high redshift galaxy distributions provides access to the evolution of the typical scale of the ionised bubble.

In this paper, we investigate the detectability of the cross-correlation between the 21 cm fluctuations and CMB by performing a signal-to-noise (SN) analysis. Particularly, we focus on the cross-correlation on large scales and we discuss the detectability of the signals and the sensitivity to the reionisation properties by Planck and LOFAR which will release useful data for the cross-correlation in the near future. This article is organised as follows. In Sec. II, we give a short description of the SN analysis. In Sec. III, we provide analytic form of the cross-correlation between the 21 cm fluctuations and the CMB anisotropy which include both CMB temperature anisotropy and CMB E -mode polarisation. In Sec. IV, we show the angular power spectrum of the cross-correlation. In Sec. V, we evaluate the the SN ratio of the cross-correlation and discuss the detectability by upcoming observations. Sec. VI is devoted to the conclusions. Throughout the paper, we use WMAP 5-year values for the cosmological parameters, i.e. $h = 0.73$ ($H_0 = h \times 100 \text{ km/s/Mpc}$), $T_0 = 2.725 \text{ K}$, $h^2 \Omega_b = 0.0223$ and $h^2 \Omega_m = 0.128$ (Komatsu et al. 2009) for a flat cosmology.

2 SIGNAL-TO-NOISE ANALYSIS

In order to investigate the detection level of the signals, a useful tool is the signal-to-noise (SN) analysis. The SN analysis not only can give the prospective detection level for the observations but also allows us to compute the optimal observational properties for an arbitrary detection level.

In order to evaluate SN ratio, first, we must estimate the error of the power spectrum of the cross-correlation. For simplicity, we assume that CMB, 21-cm fluctuations and instrumental noise are Gaussian and the foregrounds and noise of 21-cm fluctuations and CMB anisotropy are not correlated. Under these assumption, the error of the power spectrum of the cross-correlation can be rewritten as (Knox 1995)

$$\Delta C_\ell^2 = \frac{1}{(2\ell + 1)f_{\text{sky}}\Delta\ell} [(C_\ell^{21-\alpha})^2 + (C_\ell^\alpha + N_\ell^\alpha)(C_\ell^{21} + N_\ell^{21})], \quad (1)$$

where the superscript 21 stands for 21-cm fluctuations and the superscript α stands for D , the CMB Doppler anisotropy, or E , the E -mode polarisation, and C_ℓ and N_ℓ are the signal from the EoR and the noise power spectrum, respectively. In Eq. (1), $\Delta\ell$ is the size of bins within which the power spectrum data are averaged over $l - \Delta\ell/2 < l < l + \Delta\ell/2$, and f_{sky} is the sky fraction common to the two cross-correlated signals. In this paper, we consider *Planck* as CMB observation, which is almost full-sky. Therefore f_{sky} corresponds to the sky fraction of 21 cm observations which is the order of a few percents at most.

From Eq. (1), we can obtain the total SN ratio for the 21-cm cross-correlation as

$$\left(\frac{S}{N}\right)^2 = f_{\text{sky}} \sum_{\ell=\ell_{\text{min}}}^{\ell_{\text{max}}} (2\ell + 1) \frac{|C_\ell^{21-\alpha}|^2}{|C_\ell^{21-\alpha}|^2 + (C_\ell^{21} + N_\ell^{21})(C_\ell^\alpha + N_\ell^\alpha)}. \quad (2)$$

In the next section, we discuss the cross-correlation signal from reionisation and we explicit the noise power spectrum in Sec. 5.1.

3 FORMALISM OF THE CROSS-CORRELATION

The angular power spectrum of the cross-correlation between 21 cm fluctuations and CMB has been obtained by Alvarez et al. (2006) and Tashiro et al. (2008). Here we recall the analytic form of the cross-correlation with CMB Doppler temperature anisotropy and E -mode polarisation and give a short description for our reionisation model.

3.1 21 cm line fluctuations

The observed brightness temperature of the 21 cm lines in a direction \hat{n} and at a frequency ν is given as in Madau et al. (1997) by

$$T_{21}(\hat{n}; \nu) = \frac{\tau_{21}}{(1 + z_{\text{obs}})} (T_s - T_{\text{CMB}})(\eta_{\text{obs}}, \hat{n}(\eta_0 - \eta_{\text{obs}})), \quad (3)$$

where T_{CMB} is the CMB temperature and T_s is the spin temperature given by the ratio of the number density of hydrogen in the excited state to that of hydrogen in the ground state. The conformal time η_{obs} is associated with the redshift z_{obs} and $\nu = \nu_{21}/(1 + z_{\text{obs}})$ with ν_{21} being the frequency corresponding to the 21 cm wavelength. The optical depth for the 21 cm line absorption τ_{21} is

$$\tau_{21} = \frac{3c^3 \hbar A_{10} x_H n_H}{16k\nu_{21}^2 T_s H(z)} \quad (4)$$

where n_H is the hydrogen number density and x_H is the fraction of neutral hydrogen, which is written as a function of the ionised fraction $x_e = 1 - x_H$.

According to Eqs. (3) and (4), the observed brightness temperature of the 21 cm lines will reflect baryon density fluctuations, $\delta_b \equiv (\rho_b - \bar{\rho}_b)/\bar{\rho}_b$, and fluctuations of the neutral hydrogen fraction, $\delta_H \equiv (x_H - \bar{x}_H)/\bar{x}_H$, where ρ_b is the baryon density and the symbols with a $-$ represent the background values. We can rewrite Eq. (3) in the linear approximation

$$T_{21}(\hat{\mathbf{n}}; \nu) = [1 - \bar{x}_e(1 + \delta_x)](1 + \delta_b)T_0 \approx [(1 - \bar{x}_e)(1 + \delta_b) + \bar{x}_e\delta_x]T_0, \quad (5)$$

where \bar{x}_e and δ_x are the average and the fluctuations of the ionised fraction, respectively, which are $\bar{x}_e = 1 - \bar{x}_H$ and $\delta_x = -\delta_H$ in the linear approximation, and T_0 is a normalisation temperature factor given by

$$T_0 = 23 \left(\frac{\Omega_b h^2}{0.02} \right) \left[\left(\frac{0.15}{\Omega_m h^2} \right) \left(\frac{1 + z_{\text{obs}}}{10} \right) \right]^{1/2} \left(\frac{T_s - T_{\text{cmb}}}{T_s} \right) \text{ mK}. \quad (6)$$

The spin temperature is determined by three couplings with CMB, gas and Ly- α photons. Before the reionisation, T_s is set by the balance between the couplings with CMB and gas. Then, after gas is heated by stars and QSOs and the reionisation starts T_s becomes much larger than the CMB temperature mainly by the Ly- α coupling (Ciardi & Madau 2003). In this paper, since we focus on 21 cm signals from the EoR, we assume $T_s \gg T_{\text{cmb}}$ in order to obtain T_0 .

The 21 cm line fluctuation map at a frequency ν can be described by

$$\delta T_{21}(\hat{\mathbf{n}}; \nu) = T_0 \sum_{\ell} \int \frac{dk^3}{(2\pi)^3} \sqrt{4\pi(2\ell+1)} [(1 - \bar{x}_e)(1 + F\mu^2)\delta_b - \bar{x}_e\delta_x] j_{\ell}(k(\eta_0 - \eta_{\text{obs}})) Y_{\ell}^0(\hat{\mathbf{n}}), \quad (7)$$

where we take the Fourier expansion of δ_b and δ_x with Rayleigh's formula. We also introduced the factor $(1 + F\mu^2)$ to account for the enhancement of the fluctuation amplitude due to the redshift distortion (Kaiser effect) on the 21 cm line fluctuations, $\mu = \hat{\mathbf{k}} \cdot \hat{\mathbf{n}}$ and $F = d \ln g / d \ln a$ with $g(a)$ the linear growth factor of baryon fluctuations (Bharadwaj & Ali 2004).

3.2 CMB anisotropy

As reionisation proceeds, the coupling of CMB photons and free electrons by Thomson scattering becomes strong again. As a result, Thomson scattering during reionisation produces secondary CMB temperature anisotropy and polarisation.

In the CMB temperature, the main generation mechanisms at the EoR are the Doppler effect for first order anisotropic fluctuations and the kinetic Sunyaev-Zel'dovich effect for the second order. While the former is dominant on large scales ($\ell < 1000$), the latter dominates on small scales ($\ell > 1000$). In the following, we focus on the computation of the cross-correlation power spectrum on large scales ($\ell \sim 100$). We therefore consider only the Doppler anisotropy and neglect the kinetic Sunyaev-Zel'dovich effect, although, by making this hypothesis, we underestimate the CMB temperature anisotropy generated during reionisation at $\ell \sim 1000$.

The Doppler anisotropy of the CMB temperature produced during the EoR is given by $T_D(\hat{\mathbf{n}}) = -T_{\text{cmb}} \int_0^{\eta_0} d\eta \dot{\tau} e^{-\tau} \hat{\mathbf{n}} \cdot \mathbf{v}_b(\hat{\mathbf{n}}, \eta)$ where $\dot{\tau}$ is the differential optical depth for Thomson scattering $\tau(\eta)$ in conformal time $\dot{\tau} = n_e \sigma_T a$ with the electron number density n_e , the cross section of Thomson scattering σ_T and the scale factor a normalised to the present epoch. The continuity equation for baryons gives the peculiar velocity of baryons $\mathbf{v}_{bk} = -i(\mathbf{k}/k^2) \dot{\delta}_{bk}$ where the dot represents the derivative with respect to conformal time. Finally, the Doppler anisotropy is thus given by

$$T_D(\hat{\mathbf{n}}) = T_{\text{cmb}} \int_0^{\eta_0} d\eta \dot{\tau} e^{-\tau} \int \frac{d^3 k}{(2\pi)^3} \frac{\dot{\delta}_b}{k^2} \sum_{\ell} \sqrt{4\pi(2\ell+1)} (-i)^{\ell} \frac{\partial}{\partial \eta} j_{\ell}[k(\eta_0 - \eta)] Y_{\ell}^0(\hat{\mathbf{n}}). \quad (8)$$

where as above we have taken the Fourier expansion of δ_b with Rayleigh's formula.

During reionisation, CMB polarisation is produced from the quadrupole component of CMB temperature anisotropy by Thomson scattering. The CMB polarisation can be decomposed into E and B -modes with electric- and magnetic-like parities, respectively. We focus on the dominant modes generated by scalar perturbations. According to the Boltzmann equations for CMB, the scalar perturbations produce only E -modes which are given by (Hu & White 1997)

$$E(\hat{\mathbf{n}}) = \sum_{\ell m} (-i)^{\ell} \sqrt{\frac{4\pi}{2\ell+1}} \int \frac{d^3 k}{(2\pi)^3} E_{\ell}^{(0)} Y_{\ell}^m(\hat{\mathbf{n}}), \quad (9)$$

$$\frac{E_\ell^{(0)}(\eta_0, k)}{2\ell + 1} = -\frac{3}{2} \sqrt{\frac{(\ell + 2)!}{(\ell - 2)!}} \int_0^{\eta_0} d\eta \dot{\tau} e^{-\tau} P^{(0)} \frac{j_\ell(k(\eta_0 - \eta))}{(k(\eta_0 - \eta))^2}, \quad (10)$$

where $P^{(0)}$ is the $m = 0$ source term due to Thomson scattering. It is related to the initial gravitational potential Φ_0 via the transfer function $D_E(k, \eta)$, $P^{(0)} = D_E(k, \eta)\Phi_0$; this is detailed in the appendix of Tashiro et al. (2008).

3.3 Cross-correlation between 21 cm and CMB

The angular power spectrum is defined as the average of the spherical harmonic coefficients $a_{\ell m}$ over the $(2\ell + 1)$ m -values, $C_\ell = \sum_m \langle |a_{\ell m}|^2 \rangle / (2\ell + 1)$, where the $a_{\ell m}$ are defined for an arbitrary sky map $f(\hat{n})$ as $f(\hat{n}) = \sum_{\ell m} a_{\ell m} Y_\ell^m$.

From Eqs. (7) and (8), the cross-correlation between the 21-cm line fluctuations and the CMB Doppler temperature anisotropy can be written as

$$C_\ell^{21-D}(z_{\text{obs}}) = -\frac{2}{3\pi} \int_0^\infty k^2 dk \int_0^{\eta_0} d\eta [4\bar{x}_H(z_{\text{obs}})D_b(k, \eta_{\text{obs}})k^2 P_\Phi(k) - 3\bar{x}_e(z_{\text{obs}})P_{x\Phi}] \times j_\ell[k(\eta_0 - \eta_{\text{obs}})]j_\ell[k(\eta_0 - \eta)] \frac{\partial}{\partial \eta} \dot{\tau} e^{-\tau} \dot{D}_b(k, \eta), \quad (11)$$

where P_Φ and $P_{x\Phi}$ are the power spectra of the initial gravitational potential and the cross-correlation between the gravitational potential and the fluctuations of the ionised fraction, respectively. The function $D_b(k, \eta)$ relates δ_b to the initial gravitational potential Φ_0 as $\delta_b(k, \eta) = k^2 D_b(k, \eta)\Phi_0(k)$, and we have set $F\langle\mu^2\rangle = 1/3$ for the matter dominated epoch. We can simplify Eq. (11) by using the approximation for $\ell \gg 1$: $2 \int_0^\infty dk P(k) j_\ell(kr) j_\ell(kr') / \pi \approx P(k = l/r) \delta(r - r') / l^2$. We finally obtain

$$\ell^2 C_\ell^{21-D}(z_{\text{obs}}) = -\frac{1}{3} \left(\frac{\ell}{r_{\text{obs}}} \right)^2 \left[4\bar{x}_H(z_{\text{obs}})D_b(k, \eta_{\text{obs}}) \left(\frac{\ell}{r_{\text{obs}}} \right)^2 P_\Phi \left(\frac{\ell}{r_{\text{obs}}} \right) - 3\bar{x}_e(z_{\text{obs}})P_{x\Phi} \left(\frac{\ell}{r_{\text{obs}}}, z_{\text{obs}} \right) \right] \frac{\partial}{\partial \eta'} \dot{\tau} e^{-\tau} \dot{D}_b(k, \eta)|_{\eta=\eta_{\text{obs}}}. \quad (12)$$

Eq. (12) involves two terms. One involves P_Φ and is the homogeneous ionisation term. The other term involves $P_{x\Phi}$ and is the bias term. The homogeneous term corresponds to the anti-correlation part of the signal. In over-dense regions, the 21-cm emission is strong due to the large amounts of hydrogen ($\delta_{21} > 0$); while the CMB temperature is lower due to the Doppler shift ($\delta_{\text{Doppler}} < 0$). The bias term in turn shows the positive correlation part of the signal. In over-dense regions, ionising sources are numerous and the quantity of neutral hydrogen is small. Therefore, the 21-cm emission in over-dense regions is weaker than the background emission ($\delta_{21} < 0$).

The cross-correlation between 21 cm line fluctuations and E -modes was studied in detail by Tashiro et al. (2008). We provide here the basic equation

$$C_\ell^{E-21} = -\frac{3}{\pi} T_0 \sqrt{\frac{(\ell + 2)!}{(\ell - 2)!}} \int dk \int d\eta k^2 \dot{\tau} e^{-\tau} D_E(k, \eta) \left[\frac{4}{3} (1 - \bar{x}_e) P_{\Phi\delta_b} - \bar{x}_e P_{x\Phi} \right] \frac{j_\ell(k(\eta_0 - \eta_{\text{obs}}))j_\ell(k(\eta_0 - \eta))}{(k(\eta_0 - \eta))^2}. \quad (13)$$

where $P_{\Phi\delta_b}$ is the power spectrum of the cross-correlation between the gravitational potential and the baryon density fluctuations. According to the cosmological linear perturbation theory (e.g. Kodama & Sasaki 1984) the power spectrum $P_{\Phi\delta_b}$ can be written in terms of the initial power spectrum of the gravitational potential P_Φ as $P_{\Phi\delta_b} = k^2 D_b(k, \eta)P_\Phi$. The function $D_E(k, \eta)$ exhibits an oscillatory behavior and it can be decomposed as well into a homogeneous-ionisation and a bias terms. However, their signs depend on D_E .

3.4 Reionisation model

Cross-correlations between 21 cm and CMB in Eqs. (12) and (13) involve two power spectra P_Φ and $P_{x\Phi}$. While P_Φ is computed using the WMAP cosmological parameters, $P_{x\Phi}$ depends on the reionisation process. Although the latter is not well-known, we can reasonably expect that ionising sources are formed in dense regions and that they ionise the surrounding medium with an efficiency that depends on the density of the medium. Therefore, we can distinguish two possible cases: One where ionised fluctuations and matter over-densities coincide, and the other where ionised fluctuations and matter density are anti-biased (e.g. Benson et al. 2001). Following Alvarez et al. (2006), we assume that the fluctuations of the ionised fraction are associated with the matter density contrast using the Press-Schechter description (Press & Schechter 1974). As a result, the power spectrum $P_{x\Phi}$ is given by

$$\bar{x}_e P_{x\Phi} = -\bar{x}_H \ln \bar{x}_H [\bar{b}_h - 1 - f] D_m(k, \eta) k^2 P_\Phi, \quad (14)$$

where D_m is the transfer function of matter (both dark and baryonic), \bar{b}_h is the average bias of dark matter halos more massive than the minimum mass of the source of ionising photons M_{min}

$$\bar{b}_h = 1 + \sqrt{\frac{2}{\pi}} \frac{e^{-\delta_c^2/2\sigma^2(M_{\text{min}})}}{f_{\text{coll}}\sigma(M_{\text{min}})}, \quad (15)$$

where $\sigma(M)$ is the variance of the density fluctuations smoothed with a top-hat filter of the scale corresponding to a mass M , and f_{coll} is the fraction of matter collapsed into halos with $M > M_{\text{min}}$. In this paper, we choose M_{min} such that the halo virial temperature is $T_{\text{vir}}(M_{\text{min}}) = 10^4$ K. This choice corresponds to the assumption that the ionising sources form in dark matter halos where the gas cools efficiently via atomic cooling. The parameter f describes the reionisation regime we are interested in. For $f = 0$, we are in the “photon-counting limit” case where recombinations are not important and where the progress of the reionisation depends on the number of ionising photons only. The over-dense regions contain more collapsed objects which are sources of ionising photons. Therefore, in this case, ionisation in over-dense regions is easier than in under-dense regions. On the contrary, $f = 1$ indicates the “Strömgren limit” case where ionisation is balanced by recombination. Although the over-dense regions contain more sources of ionising photons, the recombination rate in over-dense regions is higher than in under-dense regions. Hence, over-dense regions in the $f = 1$ case have a lower ionised fraction than in the $f = 0$ case (for details, see Alvarez et al. 2006).

Finally, in order to calculate the cross-correlation, we need the evolution of the mean ionised fraction for which we use a simple parameterisation based on two key quantities, the reionisation redshift (defined as the redshift at which the ionised fraction equals 0.5), z_{re} , and the reionisation duration, Δz ,

$$\bar{x}_e(z) = \frac{1}{1 + \exp[(z - z_{\text{re}})/\Delta z]}. \quad (16)$$

4 CROSS-CORRELATION POWER SPECTRUM

In the left panel of Fig. 1, we show the power spectrum of the cross-correlation between the 21-cm line fluctuations and the Doppler anisotropy. For this computation, we set the reionisation redshift and duration as $z_{\text{re}} = 10$, $\Delta z = 0.1$ and we take $z_{\text{obs}} = 10$. We explore both the photon-counting-limit case ($f = 0$) and the Strömgren-limit case ($f = 1$). In both cases the cross-correlation has a positive sign. As mentioned earlier, more fluctuations are produced in the photon-counting-limit case than in the Strömgren-limit case. The amplitude of the power spectrum with $f = 0$ is thus larger than that with $f = 1$.

The cross-correlation signal has two different contributions with opposite signs as shown in Sec. 3.3. One is associated with the bias term and the other is with the homogeneous term. For reference, we plot the homogeneous ionisation part as the thin line in the left panel of Fig. 1. At high redshifts ($z > 15$), since the average bias is high, the bias part dominates the homogeneous part as shown in the model of Alvarez et al. (2006) where they have taken $z_{\text{re}} = 15$ and $z_{\text{obs}} = 15$. However, at low redshifts ($z < 15$), since the bias is the order of 1, the bias term is comparable to the homogeneous part. Therefore, in our reionisation model where $z_{\text{re}} = 10$ and $z_{\text{obs}} = 10$, cancellation occurs in the total signal. Subsequently, the total amplitude of the cross-correlation ends up smaller than that in the homogeneous ionisation part.

The right panel of Fig. 1 exhibits the dependence of the cross-correlation power spectrum on the reionisation duration for the case with $z_{\text{re}} = 10$, $z_{\text{obs}} = 10$ and $f = 0$. When the reionisation time is fixed, the shorter the duration the larger the amplitude of the power spectrum. As a matter of fact, long duration of the reionisation increases the integration range over η in Eq. (11) and thus causes cancellation of the correlation due to phase gap between the density and velocity fluctuations. Note that, according to Alvarez et al. (2006), the instantaneous reionisation gives an infinite signal (Eq. 12). However, Eq. (12) is obtained using the Limber approximation which is no more valid in a short duration reionisation. We therefore perform an exact calculation of the cross-correlations from Eq. (11).

The cross-correlation between 21-cm line fluctuations and CMB E -mode polarisation was studied in detail in Tashiro et al. (2008). The angular power spectrum depends on the polarisation source term $P(k_{\text{obs}})$, namely the quadrupole term of the CMB, at z_{obs} where k_{obs} satisfies $k_{\text{obs}} = \ell/(\eta_0 - \eta_{\text{obs}})$. Accordingly, the angular power spectrum exhibits its first peak at a multipole $\ell < 10$ which corresponds to the angular separation of the quadrupole at z_{obs} . The free streaming of the quadrupole at redshifts higher than z_{obs} produces oscillations at higher ℓ modes ($\ell > 10$). These oscillations are increasingly damped by larger reionisation durations Δz . In addition and similarly to the cross-correlation between 21-cm line fluctuations and CMB Doppler temperature anisotropy, the parameter f affects the amplitude of the cross-correlation with the E -modes. The $f = 0$ case produces more fluctuations than the $f = 1$ case, and thus a larger overall amplitude.

5 DETECTION OF THE CROSS-CORRELATION SIGNALS

For computation of the SN ratio, evaluating the noise power is crucial. Especially, the estimation of the experimental noise power spectrum for each observation strategy is an important factor of the noise power spectrum. Here, we introduce the parameterisation of the experimental noise for the various planned observation: LOFAR, MWA, SKA. Then, we calculate the SN ratio for the 21 cm cross-correlation with CMB Doppler temperature and CMB E -mode polarisation which are given by Eqs. (12) and (13), respectively.

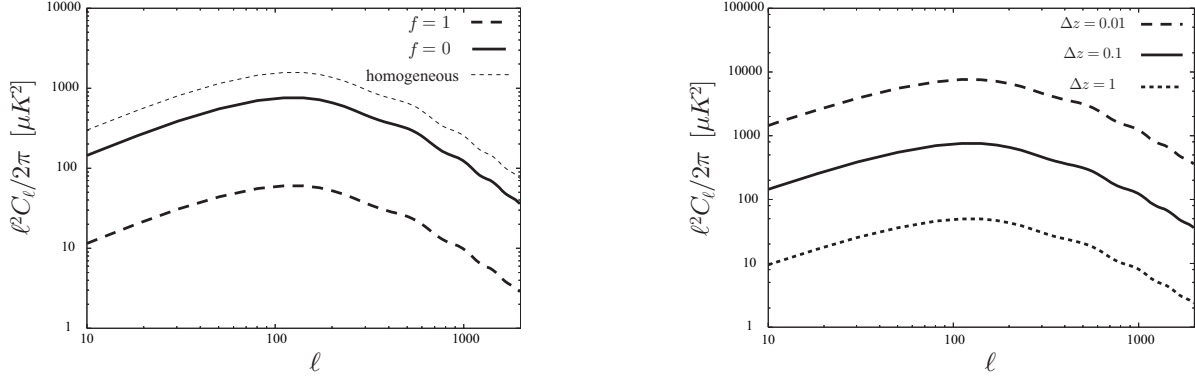


Figure 1. The cross-correlation between 21-cm fluctuations and CMB Doppler temperature anisotropy. In the left panel, we show the dependence on the reionisation model. We set $z_{\text{re}} = 10$, $\Delta z = 0.1$ and $z_{\text{obs}} = 10$. The solid line represents the $f = 0$ case where we do not take into account the recombinations. The dashed line is for the $f = 1$ case where recombinations and ionisations are balanced. The thin dotted line represents the homogeneous term where we do not consider the fluctuations of the ionised fraction δ_x . In the right panel, the dependence on the reionisation duration is shown for $z_{\text{re}} = 10$, $f = 0$ and $z_{\text{obs}} = 10$. The dashed, solid and dotted lines are for $\Delta z = 0.01$, $\Delta z = 0.1$ and $\Delta z = 1$, respectively.

5.1 Noise power spectrum

In order to evaluate the noise power spectrum, we neglect the foregrounds. Under this assumption, the noise power spectrum of the signal from reionisation consists of the experimental noise power spectrum and of the power spectrum of primary CMB.

For the CMB observation, we consider the *Planck* configuration. In this case, compared with the CMB signal, the experimental noise is very small on scales of interest. Therefore, we neglect the experimental noise power spectrum. This assumption gives the noise for the CMB Doppler temperature anisotropy as $N_\ell^D = C_\ell^T$ and for E -mode polarisation from reionisation as $N_\ell^E = C_\ell^E$ where C_ℓ^E is the primary CMB E -modes.

For the 21-cm fluctuations, the dominant signal of the 21-cm line on large scales is that of reionisation. Therefore, we can assume that the noise spectra of the 21-cm fluctuations consist of the experimental noise power spectra only. According to Zaldarriaga et al. (2004), the power spectrum of the experimental noise of the 21-cm observations at a wavelength λ cm is given by

$$\frac{\ell^2 N_\ell^{21}}{2\pi} = \left(\frac{\ell}{100} \right)^2 N_{100}, \quad (17)$$

where N_{100} is a normalised noise power spectrum which is written as

$$N_{100} = \frac{1}{t_{\text{obs}} \Delta \nu} \left(\frac{100 \ell_{\text{max}}}{2\pi} \frac{\lambda^2}{A/T} \right)^2. \quad (18)$$

Here $\Delta \nu$ is the bandwidth, t_{obs} is the total integration time, A/T is the sensitivity (an effective area divided by the system temperature) and $\ell_{\text{max}} = 2\pi \frac{D}{\lambda}$ is the maximum multipole associated with the length of the baseline D . In Table 1, we summarise the main characteristics of the present designs of MWA (Bowman et al. 2006; Lidz et al. 2008), LOFAR (Jelić et al. 2008) and SKA (Alvarez et al. 2006) and calculate $\sqrt{N_{100}}$ for the observation wavelength corresponding to an observing redshift $z_{\text{obs}} = 10$ matching the present reionisation limits. In the table, LOFAR-1 and LOFAR-3 stand for two cases one with a single observed field, LOFAR-1, and the second with the three observed fields, LOFAR-3. For reference, we consider an ideal experiment which we refer to as “super SKA” with a sensitivity 10 times that of SKA and a field of view twice as large as SKA’s.

5.2 Results

We calculate the SN ratio for the cross-correlation between 21 cm fluctuations and the CMB Doppler temperature anisotropy (Fig. 2) and CMB E -modes (Fig. 3) for a reionisation model with $z_{\text{re}} = 10$ and different reionisation durations. In both figures, we show the dependence of SN ratio on f_{sky} and N_{100} . From left to right Δz is set to 0.01, 0.1 and 0.5. In these two-parameter-space figures, we show the positions of the current experimental designs for 21 cm observations (see also Table 1). Fig. 2 shows that the cross-correlation between Planck and LOFAR, in its present configuration, is only sensitive to an “instantaneous” reionisation (with $\Delta z = 0.01$). If the quantity N_{100} , expressing the instrumental noise of LOFAR, were reduced by a factor ten (by improving the sensitivity T/A or increasing the observation time t_{obs}), LOFAR would detect the cross-correlation signal from the instantaneous reionisation with $S/N > 3$ for single observation field and $S/N > 5$ for multi observation fields. As shown in Sec. 4, the longer the duration of reionisation Δz , the smaller the amplitude of the cross-correlation. As a result,

	f_{sky}	$\Delta\nu$ (MHz)	t_{obs}	A/T (m^2/K)	D (Km)	$\sqrt{N_{100}}$ (μK)
MWA	0.02	6	1000 hour	13	1.5	5600
LOFAR-1	0.0024	1	800 hour	108	2	1200
LOFAR-3	0.007	1	1500 hour	108	2	900
SKA	0.009	1	1 month	1000	1	140
super SKA	0.018	1	1 month	1000	1	70

Table 1. The current designs of 21 cm experiments. The estimated $\sqrt{N_{100}}$ is computed for the observation wavelength which corresponds to $z_{\text{obs}} = 10$.

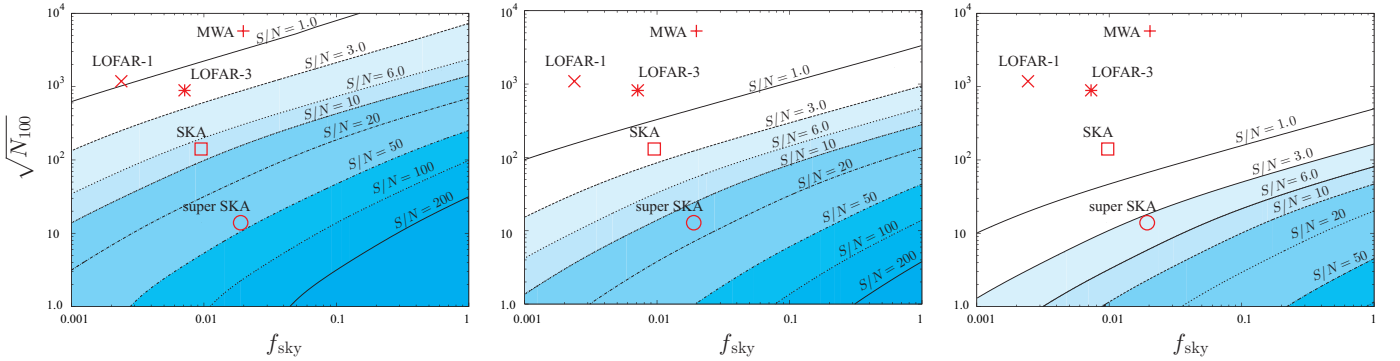


Figure 2. SN ratio of the 21-cm cross-correlation with the CMB Doppler anisotropy for different reionisation durations. In all panels, the SN ratio is given as a function of the sky fraction f_{sky} and the normalised noise power spectrum N_{100} . In all panels, we set $z_{\text{obs}} = 10$ and $z_{\text{re}} = 10$. From left to right, the reionisation durations are set to $\Delta z = 0.01$, $\Delta z = 0.1$ and $\Delta z = 0.5$.

LOFAR becomes insensitive to the reionisation signal for $\Delta z = 0.1$ whereas SKA sees the signal-to-noise decreasing from $S/N = 8$ when $\Delta z = 0.01$ to $S/N = 2.5$ when $\Delta z = 0.1$. When the reionisation is longer, $\Delta z = 0.5$, the cross-correlation signal is detected only by an ideal experiment like “super SKA”.

Fig. 3 shows that the cross-correlation signal is detected only by an ideal experiment like “super SKA” with at most $S/N = 1.0$. We show, in Fig. 4, the cross-correlation power spectrum between 21 cm and CMB E -modes with the errors estimated from Eq. (1). As mentioned previously, increasing the duration of reionisation damps the power at high ℓ s. At those scales, the noise due to CMB signal dominates the cross-correlation signal making it very difficult to probe the duration of reionisation (see Fig. 4). As a result, the SN ratio does not depend on Δz as shown in Fig. 3.

The amplitude of the cross-correlation gradually increases as the redshift z_{obs} goes down. The signal reaches its maximum value at $z_{\text{obs}} = z_{\text{re}}$ where the ionised fraction is about one half. Tracing this evolution in the cross-correlation signal with future radio-interferometer observations may possibly constrain the duration of reionisation. This is illustrated in Fig. 5, where we show the cross-correction with the estimated error at different redshifts in the ideal case of *super SKA* for two different reionisation durations, $\Delta z = 0.1$ and $\Delta z = 0.5$. We show that the signal from the instantaneous reionisation $\Delta z = 0.01$ vanishes before or after the redshift z_{re} , whereas the signal from a longer duration, $\Delta z = 0.5$, does not disappear.

In the estimation of the SN ratio of the cross-correlation, the auto-correlation for each observation is the ultimate source of noise as shown in Eq. 2. We therefore calculate the highest SN ratio attainable, i.e. in the full sky survey (the sky fraction is a multiplicative factor), and we plot the resulting SN ratio as a function of N_{100} in Fig. 6. For this computation, we set $z_{\text{obs}} = 10$ and $z_{\text{re}} = 10$ and $f = 0$. The amplitude of the 21-cm cross-correlation with the CMB Doppler anisotropy depends on the reionisation duration. Therefore, the critical value of N_{100} , where the 21-cm auto-correlation-term (C_{ℓ}^{21}) dominates the 21-cm experimental noise (N_{ℓ}^{21}), depends as well on the reionisation duration. The critical value for $\Delta z = 0.01$ is $N_{100} \sim 1.0$ and that for $\Delta z = 1.0$ is $N_{100} \sim 0.1$. Since the 21-cm cross-correlation with the CMB Doppler anisotropy has a sufficiently high amplitude and a peak at large scales, it can be detected by present or planned experiments (Fig. 6 left panel). For the 21-cm cross-correlation with the CMB E -mode polarisation, although the long duration of reionisation damps the power at high ℓ s, the noise which dominates the cross-correlation signal at these scales makes it difficult to probe the duration. Therefore, the difference due to the duration does not prominently appear in the right panel of Fig. 6. The critical value of N_{100} is same for different reionisation durations (the critical value is $N_{100} \sim 1.0$). Regardless of the duration of reionisation, the signal of the cross-correlation can be detected with an SN ratio larger than 10.

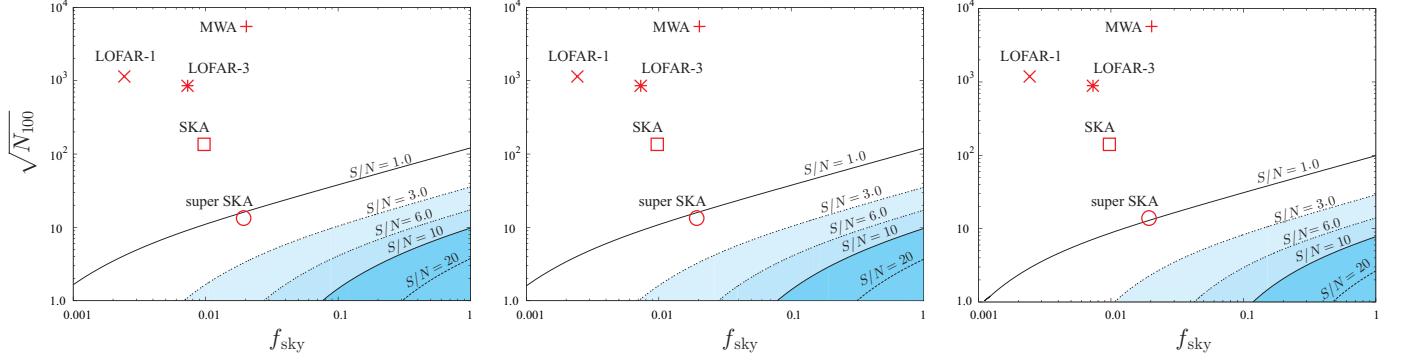


Figure 3. SN ratio of the 21-cm cross-correlation with the CMB E -modes for different reionisation durations. In all panels, the SN ratio is given as a function of the sky fraction f_{sky} and the normalised noise power spectrum N_{100} . In all panels, we set $z_{\text{obs}} = 10$ and $z_{\text{re}} = 10$. From left to right, the reionisation durations are set to $\Delta z = 0.01$, $\Delta z = 0.1$ and $\Delta z = 0.5$.

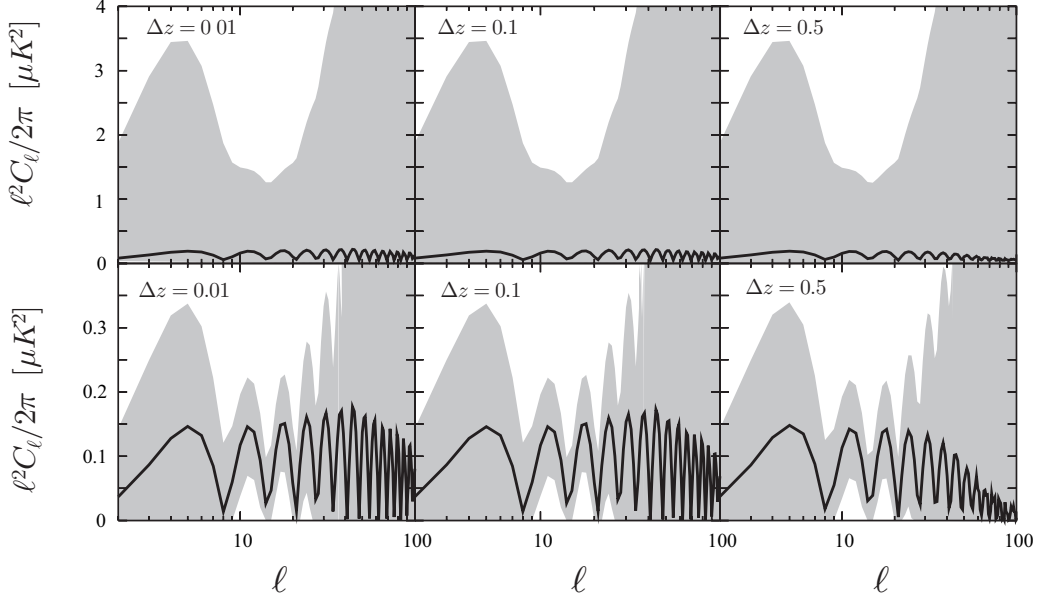


Figure 4. The 21-cm and E -mode cross-correlation signal with the estimated errors. We set $z_{\text{obs}} = 10$, $z_{\text{re}} = 10$ and $f = 0$. From the left to the right, we take $\Delta z = 0.01$, 0.1 and 0.5 . The top panels show the cross-correlation error for SKA and, the bottom panels are for *super SKA*. The cross-correlation signal is the solid line and the error regions are represented as the gray zone in each panel.

6 CONCLUSION

We have investigated the detection level of the cross-correlation between 21-cm fluctuations and large scale CMB anisotropy from the EoR. We have evaluated the signal-to-noise (SN) ratio for the 21 cm cross-correlation with both the Doppler temperature anisotropy and the E -mode polarisation. During the EoR, CMB anisotropies are also produced by patchy reionisation and Ostriker-Vishniac effect. These anisotropies also cross-correlate with 21 cm fluctuations, on small scales (Salvaterra et al. 2005; Cooray 2004; Slosar et al. 2007; Jelic et al. 2009). However on such scales, the CMB anisotropy is contaminated by other secondary effects from galaxy clusters, e.g. Sunyaev-Zeld’vich effect, which has a cross-correlation with 21-cm fluctuations (Slosar et al. 2007). The detection of the cross-correlation signal from EoR at small scales is beyond the scope of the present study. We will address this issue in a forthcoming paper.

For the cross-correlation between the 21-cm fluctuations and the CMB Doppler anisotropy produced during the EoR, the amplitude of the spectrum depends on the reionisation duration. Short durations imply high amplitude of the cross-correlation, and consequently large SN ratio. The cross-correlation between Planck and LOFAR, in its present configuration, is sensitive to an “instantaneous” reionisation (with $\Delta z = 0.01$) only. If the instrumental noise of LOFAR were reduced by a factor ten, LOFAR could detect the cross-correlation signal from the instantaneous reionisation with $S/N \sim 3$ for single observation field and $S/N \sim 5$ for multi observation field. Moreover, an ideal experiment with a sensitivity 10 times better and a field of view twice as big as that of SKA can detect the signal from the reionisation with $\Delta z = 0.5$.

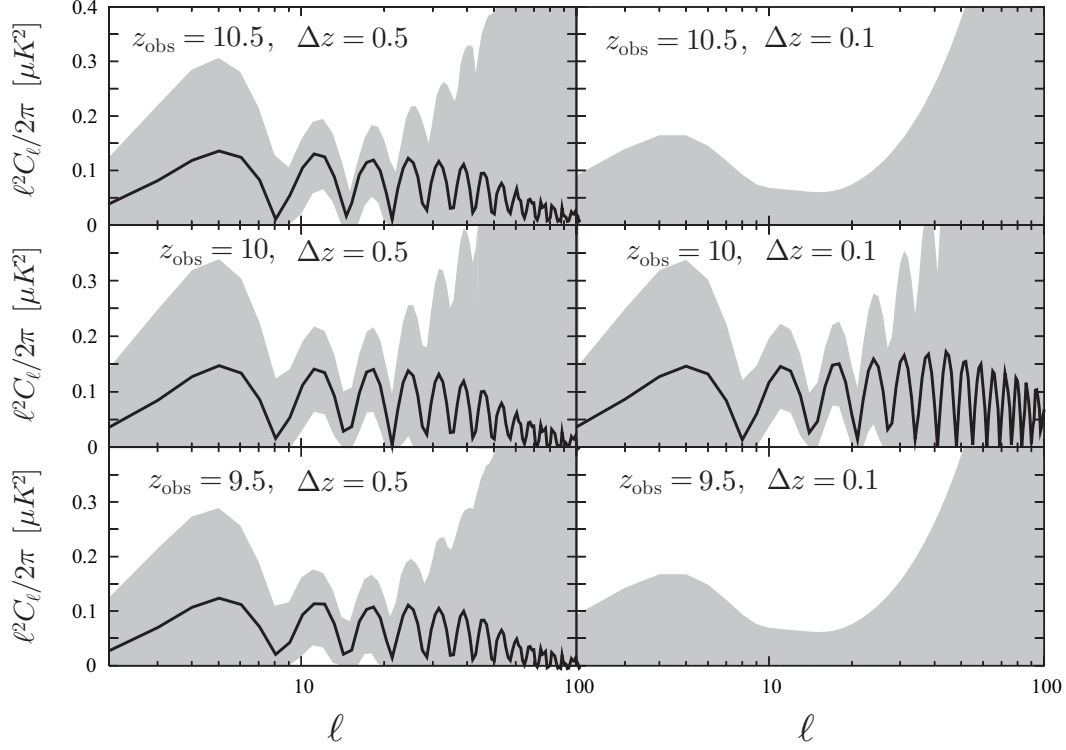


Figure 5. The 21-cm and E -mode cross-correlation signal with the estimated errors, for SKA, at different observing redshifts. We set $z_{\text{re}} = 10$ and $f = 0$ with $\Delta z = 0.5$ and $\Delta z = 0.1$ in the left and right panels, respectively. From top to bottom, we set $z_{\text{obs}} = 10.5, 10$ and 9.5 . The cross-correlation signal is shown as the solid line and the errors are represented as the gray zone in each panel.

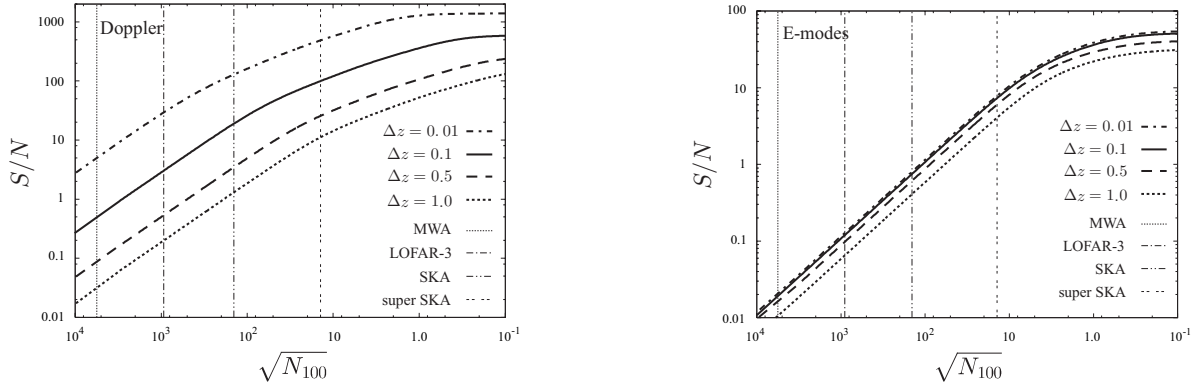


Figure 6. The SN ratio as a function of N_{100} for the ideal full sky survey. We set $z_{\text{re}} = 10$, $f = 0$ and $z_{\text{obs}} = 10$. The dashed-dotted, solid, dashed and dotted lines are for $\Delta z = 0.01, \Delta z = 0.1, \Delta z = 0.5$ and $\Delta z = 1$, respectively. The vertical lines represent the normalised noise power spectra for each observation. The left panel shows the SN ratio for the 21-cm cross-correlation with the CMB Doppler anisotropy, and the right panels is for the 21-cm cross-correlation with E -mode polarisation.

For the cross-correlation between the 21-cm fluctuations and the CMB E -mode polarisation, the angular power spectrum is damped on small scales by the reionisation duration. On those scales, the noise from the primordial CMB polarisation dominates the cross-correlation signal and makes the measurement of the cross-correlation insensitive to the reionisation duration. However, instead of the measurement of the damping, the signal detection over several frequencies by an ideal experiment 10 times more sensitive than SKA may give constraints on the reionisation duration.

REFERENCES

- Adshead P., Furlanetto S., 2007, arXiv:0706.3220
 Alvarez M. A., Komatsu E., Doré O., Shapiro P. R., 2006, *Astrophys. J.*, 647, 840

- Barkana R., Loeb A., 2001, *Phys. Rep.*, 349, 125
- Benson A. J., Nusser A., Sugiyama N., Lacey C. G., 2001, *MNRAS*, 320, 153
- Bharadwaj S., Ali S. S., 2004, *MNRAS*, 352, 142
- Bowman J. D., Morales M. F., Hewitt J. N., 2006, *Astrophys. J.*, 638, 20
- Ciardi B., Ferrara A., 2005, *Space Science Reviews*, 116, 625
- Ciardi B., Madau P., 2003, *Astrophys. J.*, 596, 1
- Cooray A., 2004, *Phys. Rev. D*, 70, 063509
- Fan X., Carilli C. L., Keating B., 2006, *Annual Review of Astronomy & Astrophysics*, 44, 415
- Furlanetto S. R., Lidz A., 2007, *Astrophys. J.*, 660, 1030
- Furlanetto S. R., Zaldarriaga M., Hernquist L., 2004, *Astrophys. J.*, 613, 1
- Hu W., White M., 1997, *Phys. Rev. D*, 56, 596
- Jelic V., et al., 2009, *arXiv:0907.5179*
- Jelić V., et al., 2008, *MNRAS*, 389, 1319
- Knox L., 1995, *Phys. Rev. D*, 52, 4307 78, 1
- Kodama H., Sasaki M., 1984, *Progress of Theoretical Physics Supplement*, 78, 1
- Komatsu E., et al., 2009, *Astrophys. J. Supp.*, 180, 330
- Lidz A., Zahn O., Furlanetto S. R., McQuinn M., Hernquist L., Zaldarriaga M., 2009, *Astrophys. J.*, 690, 252
- Lidz A., Zahn O., McQuinn M., Zaldarriaga M., Hernquist L., 2008, *Astrophys. J.*, 680, 962
- Madau P., Meiksin A., Rees M. J., 1997, *Astrophys. J.*, 475, 429
- Press W. H., Schechter P., 1974, *Astrophys. J.*, 187, 425
- Salvaterra R., Ciardi B., Ferrara A., Baccigalupi C., 2005, *MNRAS*, 360, 1063
- Slosar A., Cooray A., Silk J. I., 2007, *MNRAS*, 377, 168
- Tashiro H., Aghanim N., Langer M., Douspis M., Zaroubi S., 2008, *MNRAS*, 389, 469
- Tozzi P., Madau P., Meiksin A., Rees M. J., 2000, *Astrophys. J.*, 528, 597
- Wyithe J. S. B., Loeb A., 2007, *MNRAS*, 375, 1034
- Zaldarriaga M., Furlanetto S. R., Hernquist L., 2004, *Astrophys. J.*, 608, 622